B. CHEN
Y. CHEN
J. SIMMONS
T.Y. CHUNG
M. BASS[✉]

# Thermal Lensing
# of Edge-pumped Slab Lasers-I

College of Optics and Photonics/CREOL/FPCE, University of Central Florida, Orlando, FL 32816, USA

**ABSTRACT** We present realistic calculations of thermal lensing in edge-pumped, $Yb^{3+}$ doped yttrium aluminum garnet (YAG), slab lasers for both straight-through and zigzag propagation. Using ray tracing and finite element analysis we simulate the distributions of absorbed pump power, temperature, and stress. From these results we numerically calculate the induced lensing due to thermal and stress gradients. Effects on induced lensing of gaps in the diode pump source array and due to bonding undoped host crystal to the slab edges are presented.

**PACS** 42.55.Rz; 42.55.Wd; 42.60.Lh

## 1 Introduction

Due to pump induced volumetric heating and surface cooling of the laser material, high-average-power solid-state lasers suffer from thermally induced optical distortions. These thermal effects, including stress fracture, stress-induced birefringence, and thermal lensing, are the main limiting factors to the laser power and beam quality that can be achieved. As such, they are also some of the most critical issues to be considered in the development of high-power solid-state lasers. Discussions of thermal lensing based on assumptions allowing analytical solutions can be found in [1] and other such texts. In our earlier work we reported the stress fracture and thermal gradient induced stress birefringence in crystalline slab lasers [2–4]. In this article, we address thermal lensing in this type of laser using numerical techniques to treat the realistic three dimensional slab that reveal important properties not evidenced in analytical models.

The maximum pump-power range $\Delta P_{\text{p,max}}$ for stable laser oscillation is given for rod lasers in [5] as

$$\Delta P_{\text{p,max}} = (2M^2 - 1)\frac{4\lambda}{D^*} , \tag{1}$$

where $M^2$ is the beam propagation factor and $\lambda$ denotes the wavelength. $D^*$ is the specific dioptric power of the thermal lens caused by pump intensity, $I$, $D^* = D/I_{\text{pump}}$, with $D$ being the focal power of the thermal lens of the laser. It can be

[✉] Fax: (407) 823-6880, E-mail: bass@creol.ucf.edu

seen from (1) that the specific dioptric power $D^*$ has to be reduced to make possible the use of higher pump powers while retaining good beam quality. In a qualitative sense, this principle also applies to slab lasers although (1) is derived for rod lasers. It is essential to achieving good slab laser performance to reduce thermal and stress induced lensing and make the effective $D^*$ smaller.

The performances of real slab lasers are often noticeably poorer than theoretically predicted. This is mainly due to the fact that real lasers do not satisfy the assumptions made to enable analytical calculations. The optical distortions caused by non-uniform pumping and cooling induced gradients, as well as end effects in a slab of finite extent, prove to be very important. The following factors are the main contributors to the thermal lensing in slab lasers.

- Temperature gradients: the refractive index is a function of temperature so that temperature gradients lead to different optical path lengths for different rays.
- Thermal stress: stress causes changes in refractive index due to the stress-optic effect. The magnitude of this effect depends on the polarization direction. In the present paper, polarization parallel to the thickness ($\pi$-polarization) of the slab is assumed. (This is the preferred polarization of slab lasers having Brewster angle laser light entrance and exit faces.)
- Deformation: pumping and cooling may lead to the deformation of the laser entrance and exit faces of a slab. Other possible contributions come from bulging and ripples on the largest slab faces caused by absorbed pump power non-uniformities arising from the gap between adjacent pump diode bars in an array. These deformations may cause significant variation in the optical path length.

We present in this paper, analytic and numerical calculations of lensing in edge-pumped, face-cooled $Yb^{3+}$ doped YAG slab lasers due to thermal and stress gradients. Our results demonstrate the importance of treating the slab realistically as a three dimensional object and paying careful attention to the effects of gaps between diode bars in the pump array, and the placement of undoped material on the edges of the slab. Lensing due to deformation of the ends and large faces, and the effects of placement of undoped materials at the ends of the slab will be treated in a subsequent publication.

## 2          Pump and cooling arrangement: temperature, stress, and displacement profiles

The edge-pumped slab we consider is shown in Fig. 1a with the orientations of the axes as indicated. Diode laser pump power is introduced through each mid sized face in the manner known as edge pumping [6]. Heat deposited in the slab is removed by cooling water at 10 °C, flowing on the largest faces of the slab. In our previous work [4] the slab considered had dimensions $1 \times 16 \times 80$ mm and was pumped by 8 packages of the diode arrays. In that work we did not introduce gaps between adjacent diode bars in the array. The bars are arranged one next to another along the slab length with no gaps allowed [3]. As a result, the temperature along the length was found to be very constant. In the present calculations we allow for a more realistic 1 mm gap between the diode bars in the pump array. Figure 1b shows the gap between adjacent diode bars in an array as compared to the emitter spacing within a bar.

To have 100% gain medium utilization efficiency (fill factor = 1), we now consider a $1 \times 16 \times 89.6$ mm slab with the apex angle of the Brewster end = 30.6°. In this slab all the rays experience the same number of bounces when the laser beam follows a zigzag path at an angle equal to the apex angle of the slab. Eight arrays of 17 diode bars with a 1 mm space between arrays were arranged along each of the length-thickness sides of the slab. The 17 bars were assumed to be equipped with cylinder lenses to focus and aim the pump light

so that there would be 17 lines of diode light directed into each length-thickness edge of the slab, as shown schematically in an end on view in Fig. 1c. The output power of each pump diode bar was taken to be 40 W resulting in a total pump power of 10.88 KW.

The absorbed pump power distributions calculated using the non sequential ray tracing program ASAP [7] are shown in Fig. 2a and b. With the diode bars central wavelength set at 941 nm we assumed a 3 nm wide (full width at half maximum) Gaussian spectral distribution of the pump array output. The absorbed pump power density profiles on the length-thickness planes are relatively uniform although there are ripples at different positions in the slab length due to the gaps between adjacent bars. Our thermal lensing calculations show that these ripples do not significantly affect lensing due to temperature gradient and stress. However, such ripples do affect the lensing due to surface deformation as we will discuss in a subsequent paper.

The pump power density varies along the slab width due to edge pumping. In addition, variations of the pump light delivered to the slab exist near the end faces since the pump array
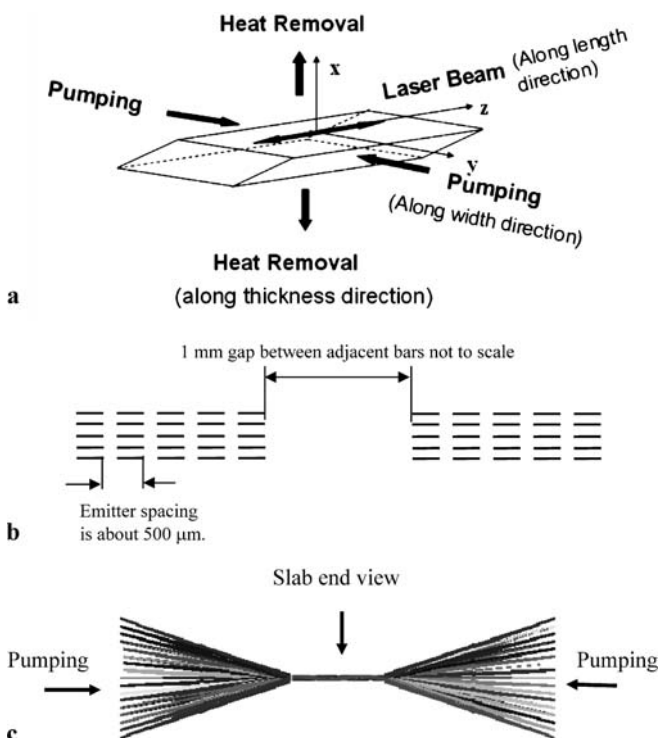


FIGURE 1  (a) Pump and cooling configuration. Pumping is through slab edges while heat is removed from the top and bottom, the largest surfaces (b) Schematic sketch of the diode array showing the gap between adjacent bars and the spacing of the emitters within a bar. (c) Sketch of the 17 rows of diode bars pumping each edge of the considered slab seen from a point on the $z$ axis looking back towards the slab
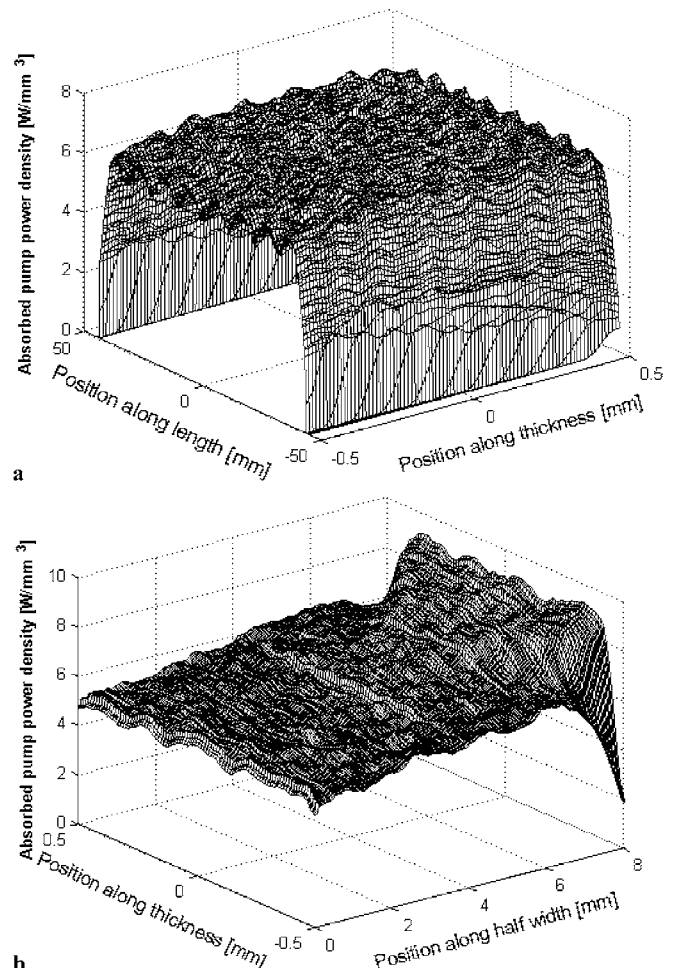


FIGURE 2  The absorbed pump power density distribution: (a) in the length-thickness plane that is 4 mm from the center of the slab in the width, and (b) in the width-thickness plane located at the mid plane in the slab length. (The locations in the slab for the sections used in (a) and (b) are indicated in Fig. 3) The small variations seen in the thickness direction in (a) and (b) are due to the magnified scale and to the voxel size used in ASAP

is only as long as the rectangular parallelepiped region of the slab. Therefore thermal gradients always exist near the ends of realistic, three dimensional, edge pumped slabs.

We performed 3D thermal and stress computations by finite element analysis (FEA) with the software program FEMLAB [8]. We used FEA to solve the heat conduction equation

$$\nabla \cdot (\nabla T) + \frac{Q}{k(T)} = 0 \tag{2}$$

with boundary conditions,

$$\frac{\partial T}{\partial x} = \frac{h_t}{k(T)} (T_{\infty t} - T_t) \quad \text{at} \quad x = \pm \frac{t}{2} \tag{3}$$

$$\frac{\partial T}{\partial y} = \frac{h_w}{k(T)} (T_{\infty} - T_w) \quad \text{at} \quad y = \pm \frac{w}{2} \tag{4}$$

$$\frac{\partial T}{\partial z} = \frac{h_l}{k(T)} (T_{\infty} - T_l) \quad \text{on the end faces} \tag{5}$$

where

$h_w, h_l$ = free convection heat transfer coefficient on edge/end faces, 5 W/m$^2$ C

$h_t$ = forced convection heat transfer coefficient on top and bottom faces, 30 000 W/m$^2$ C

$T_{\infty}$ = ambient room temperature (20 °C),

$T_{\infty t}$ = coolant temperature (10 °C), and

$T_t, T_w, T_l$ = the temperature of slab top and bottom surfaces, edge faces, and end faces, respectively, in K. The heat energy deposited per unit volume, $Q$, is a function of position in the laser medium. In our work it is taken as proportional to the absorbed pump power density distribution obtained by 3D ray tracing using ASAP. For Yb:YAG that means that 11% [9] of the absorbed pump power is taken as the heat deposited. Due to the symmetry of heat flow in the slab the thermal analysis only had to be carried out for a quarter of the slab. The temperature profile is shown in Fig. 3. Along the width of the slab the temperature increases when going outwards from the center due to the fact that the material near the edges absorbs more pump power. Along the thickness the temperature decreases going outward from the center since the large surfaces are cooled.

All components of the stress tensor responsible for thermal gradient stress induced lensing were then calculated by finite element analysis in FEMLAB. Figure 4 shows the distributions of stress components in the slab we consider. As discussed in [13] the small scale variations in Fig. 4 are due to the meshing used in the finite element analysis. According to the theory of elasticity, in a thin slab the shear stress components $\sigma_{xy}$, $\sigma_{yz}$ and $\sigma_{xz}$ and the principal stress component along the thickness direction $\sigma_{xx}$ should be very small. Our calculations show that this is true for these stresses in the central part of the slab where the approximations made to obtain the analytical results apply. However, near the slab edges and ends these stresses are large. For example, near the edges $\sigma_{xx}$ can be on the order of $10^7$ Pa. The principal stress components along slab width $\sigma_{yy}$ and length $\sigma_{zz}$ have values on the order of $10^7$ Pa. From the
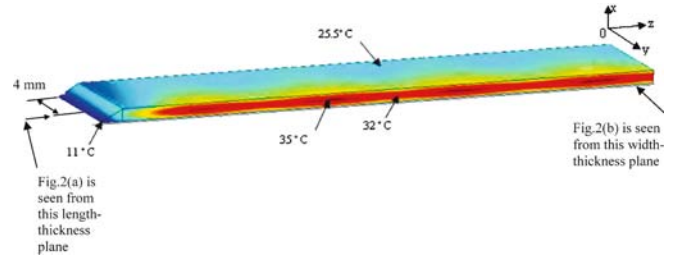

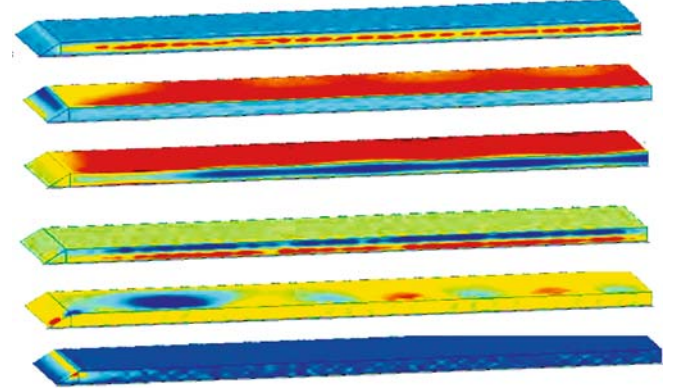
**FIGURE 3**  Temperature profile in a quarter of the slab



**FIGURE 4**  The calculated distribution of stress components, $\sigma_{xx}$, $\sigma_{yy}$, $\sigma_{zz}$, $\sigma_{xy}$, $\sigma_{yz}$, $\sigma_{xz}$, for a fully doped Yb:YAG slab of $1 \times 16 \times 89.6$ mm. Note that different color scales are used in different plots

distribution of $\sigma_{yy}$ and $\sigma_{zz}$ in Fig. 4 we see that stress near the center is compressive while near the surfaces it is tensile. The stress components, $\sigma_{yy}$ and $\sigma_{zz}$, do not vary significantly along the width and length directions inside the slab. Due to the presence of the slab boundaries $\sigma_{yy}$ and $\sigma_{zz}$ experience large gradients near the slab edges and ends. There is also a compressive to tensile change of shear stress $\sigma_{yz}$ near the edge along the length of the slab due to the gap between adjacent bars in the pump array.

## 3    Analytical calculation of thermal lensing

Excluding end effects, the focal length of the thermal lens along the width direction $F_w$, which is the inverse of dioptric power $D$, is given in (6) [10]. The focal length along the thickness direction $F_t$ is zero since uniform pumping and zig-zag propagation are assumed in [10],

$$\frac{1}{F_w} = -\frac{\eta_h \eta_{abs} (\alpha w)^3 P_p l_{eff}}{L w^2 \alpha_r \sinh(0.5 \alpha w)} \left( \frac{dn}{dT} \frac{1}{24k} - B \frac{(\alpha w)^2}{1440 M_s \alpha_r^2} \right) \tag{6}$$

where

$\alpha_r$:  aspect ratio $w/t$,

$\alpha$ :  absorption coefficient,

$P_p$:  pump power,

$\eta_{abs}$:  fraction of incident pump power absorbed,

$\eta_h$:  fraction of absorbed pump power deposited as heat,

$k$:  thermal conductivity,

$l_{eff}$:  effective length of a zigzag slab,

$M_s$:  material constant and

$B$:  constant related to stress-optical properties of materials.

| Inverse thermal focal length $1/F_{\mathrm{w}}$(1/m) | -0.078 |
|---|---|
| Dimensional ratios, $w/t$ and $l/t$ | 16, 89.6 |
| Pump power, $P_{\mathrm{p}}$(kW) | 10.88 |
| Absorption efficiency, $\eta_{\mathrm{abs}}$ (%) | 80 |
| Absorption coefficient, $\alpha$ (1/cm) (1.2 at. %) | 3.46 |
| Fraction of absorbed pump power deposited as heat, $\eta_{\mathrm{h}}$(%) | 11 |
| Thermal conductivity, $k$ (W/mK) | 13 |
| Effective length of zigzag pass, $l_{\mathrm{eff}}$(m) | 0.1 |
| $M_{\mathrm{s}}$ (m$^2$/sec) | $2.45 \times 10^{-6}$ |
| $B$ (Pa$^{-1}$) | $-1.5 \times 10^{-12}$ |

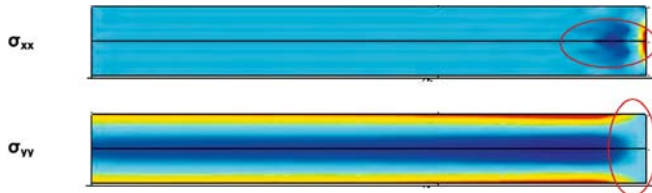**TABLE 1**    Parameters used in (6)



**FIGURE 5**    The stress distribution in the cross section of the slab

For the Yb:YAG zigzag slab laser described above we used (6) to calculate the thermal lens strength in the width direction of the slab as shown in Table 1. Comparison of this analytically calculated result with the numerically calculated values (see next sections) indicates that the analytic calculations result in too small a value for thermal focusing in finite slab lasers because the contributions of end and edge effects are not included.

In deriving the analytic expression, (6), the slab was assumed to be infinitely long. This means that the stress components including $\sigma_{zz}$ were also assumed to be uniform along the slab length. The boundary effects on stress were not included. However, this is not the case in a realistic slab where end effects contribute significantly to the thermal and stress distributions. Figure 5 shows the localized features of stress near the edges.

# 4    Numerical calculation of thermal lensing due to thermal gradients

From the 3D temperature distribution calculated using FEMLAB the refractive index changes along the light propagation paths were calculated from the known change of index with temperature for YAG. The resulting optical path length differences (OPLD) due to temperature gradients are shown in Figs. 6 and 7. Here by OPLD we mean the variations from the optical path length in the slab uniformly held at room temperature. The constant part of the optical path length doesn't affect the thermal focusing.

From the ray matrices for a lens-like medium the focal lengths of the biaxial thin lens are [11]

$$\frac{1}{F_x} = -\frac{2 \cdot (\mathrm{OPLD}(x) - \mathrm{OPLD}(x_0))}{(x - x_0)^2},$$

$$\frac{1}{F_y} = -\frac{2 \cdot (\mathrm{OPLD}(y) - \mathrm{OPLD}(y_0))}{(y - y_0)^2}. \tag{7}$$
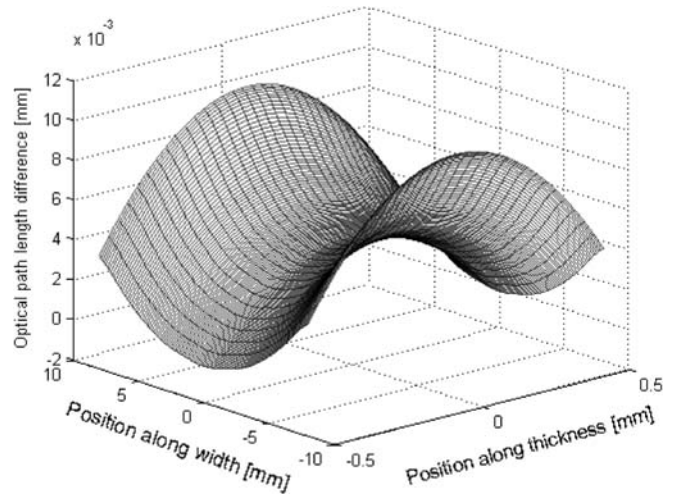


**FIGURE 6**    Optical path length difference due to thermal gradients in the case of straight through propagation
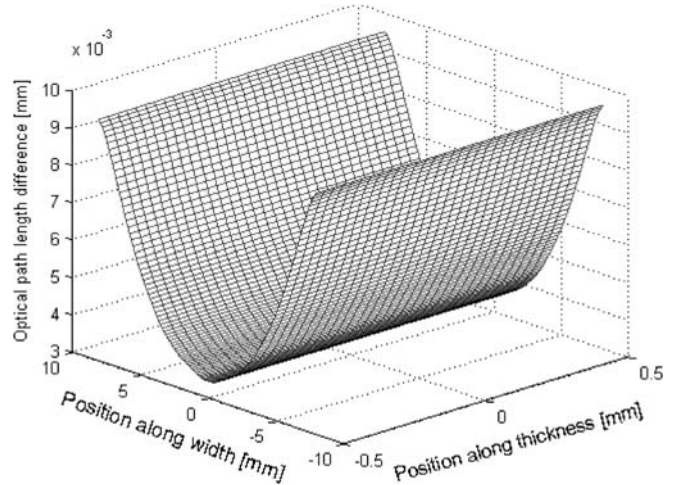


**FIGURE 7**    Optical path length difference due to thermal gradients in the case of zigzag propagation

Fitting the computed OPLD data as if it were due to a thin lens gives the equivalent focal powers as

$$\left(\frac{1}{F_t}, \frac{1}{F_w}\right) = (41.5\,\mathrm{m}^{-1},\ -0.17\,\mathrm{m}^{-1}),$$

and

$$\left(\frac{1}{F_t}, \frac{1}{F_w}\right) = (0.008\,\mathrm{m}^{-1},\ -0.19\,\mathrm{m}^{-1}) \tag{8}$$

for straight through and zigzag propagation, respectively. Here $F_t$ is the focal length in the thickness direction and $F_w$ is the focal length in the width direction. Surface cooling leads to convergent focusing along the thickness direction in the case of straight-through propagation while edge-pumping leads to divergent focusing along the width direction. In a slab in which zigzag propagation is used the focusing in the thickness direction is greatly reduced because such propagation averages out the lensing effect to first order [12].

Bonding undoped host material to the slab edges has been suggested as a means to reduce re-absorption losses [9]. The temperature distribution shown in Fig. 8 indicates that putting
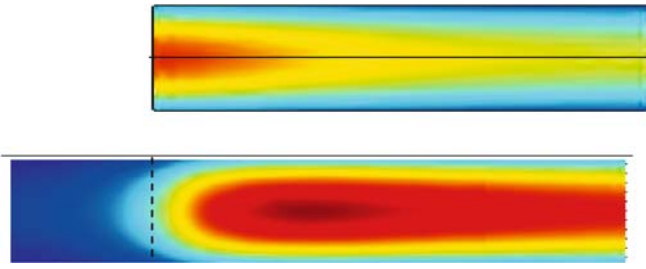
**FIGURE 8**  Temperature distribution in the cross section of a fully doped slab (*top*) and a slab with undoped crystals bonded to the edges (*bottom*)
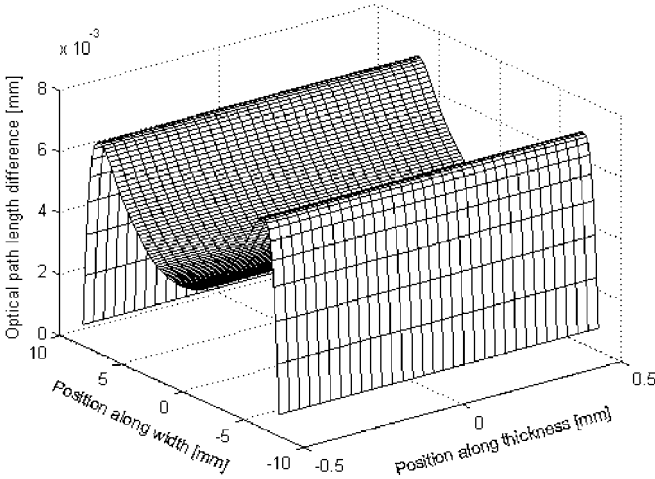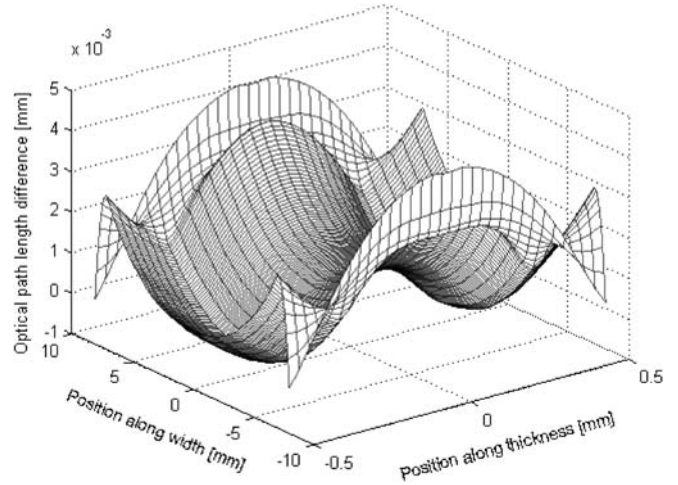


**FIGURE 10**  Optical path length difference due to thermal stress in the case of straight through propagation in the slab



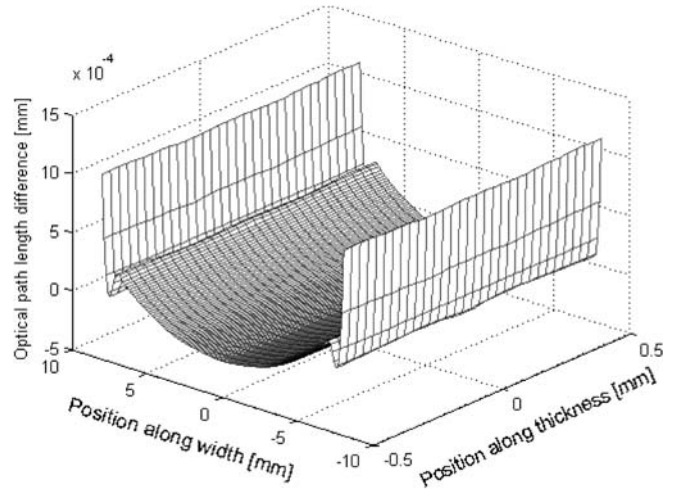**FIGURE 9**  Optical path length difference due to the thermal gradient in a zigzag slab with undoped crystalline edges



**FIGURE 11**  Optical path length difference due to thermal stress in the case of zigzag propagation in the slab

on the undoped crystalline edges causes the maximum temperature to move into the slab away from the pump light entrance edges while the maximum temperature is reduced. In such a slab the OPLD distribution due to thermal gradients is shown in Fig. 9. The resulting "M" shaped lens in the width direction may make compensation more difficult. To avoid the "M" shaped feature one could chose to restrict lasing to the central region of the slab. However, this approach means giving up a substantial part of the absorbed pump power.

## 5        Numerical calculation of thermal lensing due to stress gradients

As explained in our previous work [3, 4] the index of refraction itself cannot be treated as a tensor although it is related to tensor quantities. From the 3D stress distribution obtained with FEMLAB we calculated the changed dielectric impermeability tensor and then the changes in the refractive index due to stress. In these calculations the polarization was taken to be parallel to the thickness of the slab ($\pi$-polarization). Optical path length differences due to thermal gradient induced stresses are shown in Figs. 10 and 11. Because of boundary effects, the distribution of stress induced optical path length differences is not smooth in the case of straight-through propagation. Fitting the data as above we find the stress induced lens powers to be

$$\left(\frac{1}{F_{t}}, \frac{1}{F_{w}}\right) = (7.8\,\mathrm{m}^{-1},\ -0.082\,\mathrm{m}^{-1}),  \tag{9}$$

and

$$\left(\frac{1}{F_{t}}, \frac{1}{F_{w}}\right) = (0.006\,\mathrm{m}^{-1},\ -0.018\,\mathrm{m}^{-1})  \tag{10}$$

for straight through and zigzag propagations, respectively. As before, for straight through propagation thermal gradient induced stress leads to strong focusing in the thickness direction which is greatly reduced by employing zigzag propagation.

Bonding undoped crystals to slab edges has also been suggested as a means to reduce depolarization loss by moving the maximum stress and stress gradient out of the gain medium [4]. From Fig. 12, we can see that the localized extrema of $\sigma_{yy}$ and $\sigma_{xy}$ are moved outward when undoped material is bonded to the edges of the slab. On the other hand, the localized extrema of $\sigma_{xx}$ and $\sigma_{zz}$ are moved inward where the other two shear stress components of stress are unchanged in this example. The combined effect on the thermal lensing is shown in Fig. 13. "M" shaped lensing can be seen again but it is weaker than that due to thermal gradients.

In our previous work [3, 4] we computed the cut angle dependence of the depolarization losses in a slab that results from the fact that the dielectric impermeability tensor
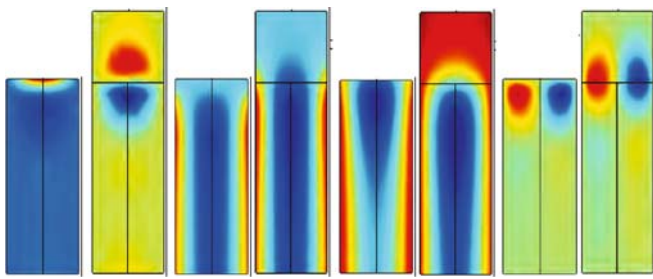
**FIGURE 12** Comparison of the distributions of $\sigma_{xx}$, $\sigma_{yy}$, $\sigma_{zz}$, $\sigma_{xy}$ (from left to right) in the cross section of a slab with and without undoped crystalline edges
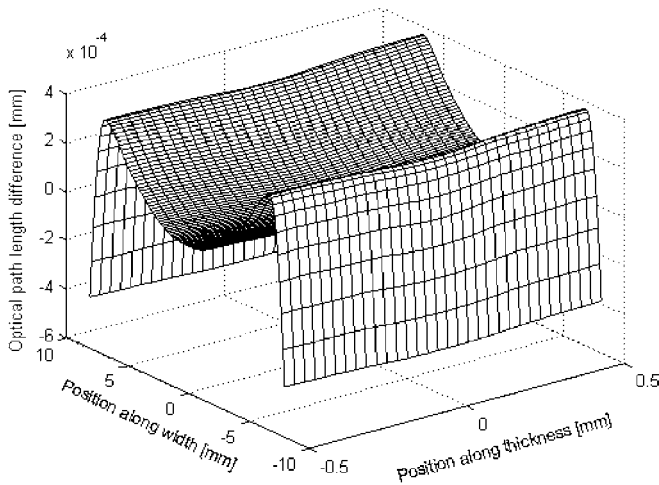


**FIGURE 13** Optical path length difference due to thermal stress in a zigzag slab with undoped crystalline edges

is cut angle dependent. Therefore it would not be surprising if the stress induced lensing were cut angle dependent. However, due to the fact the stress induced lensing is significantly smaller than the thermal gradient induced lensing, we did not explore this issue any further. In the calculations in this paper, the cut angle of slab was taken to be 0° for a fully doped slab or 30° for a slab with undoped material on the edges. These cut angles lead to minimal depolarization loss [13].

## 6    Conclusions

Using ray tracing and finite element analysis we calculated the distributions of absorbed pump power, temperature, and stress, in realistic three dimensional edge pumped slab lasers. The value of temperature or stress will differ for different size slabs with similar pumping arrangements. However, they would have similar distributions to those obtained here. From the temperature and stress distributions, we calculated the induced lensing due to thermal and stress gradients. The numerical calculations result in several generally applicable results. These include the following.

1. Thermal gradients affect thermal lensing more than thermal gradient induced stress.

2. Putting undoped edges on the edge pumped slab results in an "M" shaped feature of lensing along the slab width, making compensation with simple optics difficult.

3. The presence of gaps between bars in a pump array leads to variations in the distribution of absorbed pump power and, consequently in the temperature distribution. Such variations only minimally affect thermal lensing in an edge pumped slab but can produce thermal lensing in end pumped slabs that is difficult to correct. [14] The results of modeling the particular slab size that we considered, can be applied to any slab shaped gain medium that is edge pumped.

## REFERENCES

1 W. Koechner, *Solid-State Laser Engineering. Fifth Revised and Updated Edition* ISBN 3-540-65064-4 (Springer, NY 1999)
2 B. Chen, J. Dong, M.K.R. Patel, Y. Chen, A. Kar, M. Bass, Proc. of SPIE. **4968**, 1 (2003)
3 Y. Chen, B. Chen, M.K.R. Patel, M. Bass, IEEE J. Quantum Electron. **QE-40**, 909 (2004)
4 Y. Chen, B. Chen, M.K.R. Patel, A. Kar, M. Bass, IEEE J. Quantum Electron. **QE-40**, 917 (2004)
5 T. Graf, E. Wyss, H.P. Weber, Proc. ASSL 2001, **50**, 688 (2001)
6 T.S. Rutherford, W.M. Tulloch, S. Sinha, R.L. Byer, Opt. Lett. **26**, 986 (2001)
7 ASAP optical modeling software by Breault Research. See www.breault.com
8 A Finite Element Analysis software by COMSOL. See www.comsol.com
9 T.Y. Fan, IEEE J. Quantum Electron. **QE-29**, 1457 (1993)
10 T.S. Rutherford, Ph.D. dissertation, Stanford Univ., Stanford, CA 2001
11 J.M. Eggleston, T.J. Kane, K. Kuhn, J. Unternahrer, R.L. Byer, IEEE J. Quantum Electron. **QE-20**, 289 (1984)
12 W.S. Martin, J.P. Chernoch, US Patent 3,633,126 (January 1972)
13 Y. Chen, B. Chen, M. Bass, Appl. Phys. B **81**, 75 (2005)
14 Y. Chen, T.Y. Chung, M. Bass, 18th Ann. Solid State and Diode Laser Tech. Rev., Paper SS2-3, Directed Energy Prof. Soc., June 7–9, 2005, Los Angeles, CA